


# Brass Alloy Coatings Electrodeposited from an Environmentally Friendly Alkaline Lactate Bath under Different Operating Conditions

Medhat M. Kamel <sup>1,\*</sup> , Eman Alzahrani <sup>2</sup>, Abbass M. Abbass <sup>1</sup>, Alaa A. Abd Ellah <sup>1</sup>

<sup>1</sup> Department of Chemistry, Faculty of Science, Suez Canal University, Ismailia, 41522 Egypt; medhat\_darwish@science.suez.edu.eg (M.M.K.);

<sup>2</sup> Department of Chemistry, College of Sciences, Taif University, P.O. Box 11099, Taif 21944, Saudi Arabia; e.mohsan@tu.edu.sa (E.A.);

\* Correspondence: medhat\_darwish@science.suez.edu.eg (M.M.K.);

Scopus Author ID 36157882000

Received: 18.11.2021; Accepted: 19.12.2021; Published: 30.01.2022

**Abstract:** The electroplating of brass alloy coatings onto a steel substrate was established using a lactic acid solution under diverse practical conditions.  $\text{CuSO}_4 \cdot 5\text{H}_2\text{O}$ ,  $\text{ZnSO}_4 \cdot 7\text{H}_2\text{O}$ ,  $\text{CH}_3\text{CHOHCOOH}$ , and anhydrous  $\text{Na}_2\text{SO}_4$  were used to make the deposition bath. The impact of bath components, deposition current, as well as temperature on the current efficiency (CE) and alloy microstructure was examined. The deposition of the alloy is of the normal type. The CE is good, and it improves when the  $[\text{Zn}^{2+}] / [\text{Cu}^{2+}]$  ratio in the bath increases. On the other hand, the efficacy declines when the current density, temperature, and lactic acid concentration increase. By elevating the applied current density, or raising the concentration of the  $\text{Zn}^{2+}$  ions in the tub, the amount of Zn metal in the plated alloy is increased. SEM, energy dispersion X-ray, and X-ray diffraction techniques are being used to investigate the coating's morphology and crystal texture. The presence of copper and zinc metals in the deposit was confirmed by EDX analysis. The new bath's deposits are well-crystalline and contain a  $\text{Cu}_5\text{Zn}_8$  phase. The bath's throwing power and throwing index are determined, and it is found that the alkaline lactate tub has satisfactory throwing power and throwing index.

**Keywords:** electrodeposition; brass alloy; steel; lactic acid; coatings.

© 2022 by the authors. This article is an open-access article distributed under the terms and conditions of the Creative Commons Attribution (CC BY) license (<https://creativecommons.org/licenses/by/4.0/>).

## 1. Introduction

The term “brass” refers to a group of copper-zinc alloys. Brass comes in various qualities, but they are all strong, robust, conductive, and corrosion-resistant. Due to this, brass is one of the most widely used alloys, along with its attractive look and ease of manufacture. For centuries, brass has always been the metal of choice for many musical instruments. It is a great metal for carrying water through pipes and fittings. It is suitable for marine engines and pump components. One of the early commercial uses of brass was aboard naval ships, which is unsurprising. Because of its non-magnetic nature, the alloy is used in various ways. Components for clocks and watches, electrical terminals, and explosives require a metal that won't corrode [1].

Zinc is a very valued alloying element when combined with copper. It improves both the strength and the ductility of the material. Furthermore, zinc is less expensive than copper,

adding zinc to copper reduces material costs. Zinc may indeed reduce corrosion resistance a little, with brasses going to fall just under copper in the galvanic series.

Brass plating is primarily used for ornamental purposes, steel protection, and increasing the bonding of rubber to steel and other metals [2]. To give the impression of solid brass, decorative coatings are applied to cheap steel hardware and electrical appliances [3]. Commercially, different forms of brass are electrodeposited: yellow brass, which includes 70% Cu; white brass, which contains 30% Cu; and a rich-Cu alloy, which contains 90% Cu.

A cyanide bath is used to commercially plate brass [4]. There are various advantages to plating brass with cyanide electrolytes over other bath compositions [5]: The deposits are quite adherently. The deposit thickness is rather uniform, and the deposit morphology is fine-grained [6,7]. These baths are easy to control, resulting in thin deposits with consistent thicknesses. They have the best macro-throwing power on all surfaces [8].

The demand for a less hazardous and more stable plating bath than cyanide plating baths prompted the creation of non-cyanide brass plating baths. There are numerous scientific papers [9-36] describe the electrodeposition of brass alloys from cyanide-free baths, including pyrophosphate [9,10], citrate [11], oxalate [12], tartrate [13], EDTA [14], triethanolamine [15], ammonia [16], glucoheptonate [17], glutamate [18], and glycinate [19] baths. The electrodeposited brass could be employed as a matrix in brass composite coatings. These materials exhibit better qualities than their non-composite equivalents, such as improved tribological capabilities in the case of graphitic-brass coating [20] and increased scratch and corrosion resistance in the case of  $\text{Cu}_5\text{Zn}_8$  brass intermetallic composite coating [21].

This work attempts to develop a new cyanide-free electrolyte for brass electroplating that contains lactic acid as a complexing agent. This study aims to use an electrodeposition method to deposit brass alloy onto a steel substrate from a novel alkaline lactate bath under various operational parameters, including bath constituents, temperature, and the applied current density. The parameters impacting polarization, cathodic efficiency, throwing power (TP), throwing index (TI), and deposit structure were studied. The shape and crystal texture of the deposits have been investigated.

## 2. Materials and Methods

The deposition tests have been conducted in baths containing 0.02–0.12 M  $\text{CuSO}_4 \cdot 5\text{H}_2\text{O}$ , 0.08–0.18 M  $\text{ZnSO}_4 \cdot 7\text{H}_2\text{O}$ , 0.2 M  $\text{Na}_2\text{SO}_4$ , and 0.6–2 M lactic acid ( $\text{CH}_3\text{CHOHCOOH}$ ). Metal sulfates were kept at a total concentration of 0.20 M. The solutions were made with bi-distilled  $\text{H}_2\text{O}$  and analytical grade chemicals just before the experiments began. The pH was measured and fixed at 10 using a Fisher apparatus and was regulated by  $\text{NH}_4\text{OH}$ .

The plating cell was reported earlier [37]. It's built of Perspex and includes a steel cathode and a stainless steel (type 304) anode. The electrodes were 3 cm long and 3 cm wide. The polishing paper was used to polish the cathode abrasively. After that, it was rinsed in bi-distilled water, ethanol, and weighed. The plating process is carried out using agitated solutions. After a 30-minute plating period, the steel cathode was removed, rinsed with bi-distilled water, exsiccated, and weighed.

After digesting the coatings in 32 % HCl and diluting with bi-distilled water, the alloy compositions are determined using an atomic absorption spectrometer (Thermo, model; SOLAAR). The alloy deposition cathodic current efficacy, CE, equals the total of the parent metals' cathodic current efficacy.

$$CE = CE_{Zn} + CE_{Cu} \tag{1}$$

The following equation was used to calculate the percentage of copper metal in the alloy:

$$Cu_{(alloy)} \% = \left( \frac{\text{mass of Cu (alloy)}}{(\text{mass of Cu (alloy)} + \text{mass of Zn (alloy)})} \right) \times 100 \tag{2}$$

The percentage of zinc metal in the bath is calculated by the formula [38]:

$$Zn_{(bath)} \% = \left( \frac{\text{mass of Zn (bath)}}{(\text{mass of Cu (bath)} + \text{mass of Zn (bath)})} \right) \times 100 \tag{3}$$

The polarization tests were performed in a classic glass cell, with a steel desk with a 1 cm<sup>2</sup> area serving as the working electrode. Pt gauze was used as a counter electrode, and Ag/AgCl was used as a reference electrode. The electrodes were attached to a computer-controlled model 273 potentiostat/galvanostat system. At a scan rate 20 mV s<sup>-1</sup>, all of the tests were conducted. A circuit previously described [39] was used to determine the bath's throwing force and throwing index. The plating cell was constructed of Perspex and had internal dimensions of 20 × 3 × 2.5 cm. A single stainless steel anode was sandwiched between two parallel steel cathodes with various spacing ratios (1:1–1:3). Field's equation [40] was used to calculate the throwing power.

$$TP \% = \frac{L-M}{L+M-2} \times 100 \tag{4}$$

Where L represents the linear ratio (L = 1, 2, or 3), and M represents the metal distribution ratio ( $m_{near} / m_{far}$ ). The magnitudes of M as a function of L were measured over a range of linear ratios ranging from 1:1 to 1:3. A straight line can be constructed by graphing L vs. M. The throwing index is calculated as the line's reciprocal. It's a quick indicator of bath throwing power. SEM scanning (QUANTA FEG 250) was used to examine the surface of the deposited alloy. An X-ray apparatus (Xpert Pro P analytical, operated at 40 kV and 35 mA with Cu- K $\alpha$ ) was used to investigate the phases and crystal texture of the deposits.

### 3. Results and Discussion

#### 3.1. Potentiodynamic polarization tests.

The character of the entire electrodeposition process is influenced by cathodic polarization. It impacts the cathodic current efficacy, plating bath throwing power, and deposit quality. As a result, under various experimental conditions, cathodic potential against current density (E/i) curves for alloy deposition was recorded potentiodynamically. Figs. 1–5 illustrates cathodic polarization curves of Zn – Cu alloy deposition on steel specimens from various baths.

The relationship between current density and cathodic potentials for the deposition of Zn, Cu, and Zn–Cu alloy under identical conditions is depicted in Fig. 1. Due to the complexation with lactate anions, the polarization of the copper and zinc reduction processes moved to greater cathodic overpotentials values. The data in the graph show that the polarization curve for individual Cu metal deposition is nobler than that of Zn. The alloy's deposition curve is significantly more positive than the parent metals, zinc, and copper. This position suggests that a significant decrease in free energy accompanies the co-deposition. Zinc exists in solution as [Zn (C<sub>3</sub>H<sub>5</sub>O<sub>3</sub>)<sub>2</sub>] complex (log  $K_f$  = 2.70). Copper is present as [Cu (C<sub>3</sub>H<sub>5</sub>O<sub>3</sub>)<sub>2</sub>] complex (log  $K_f$  = 4.66) [41].

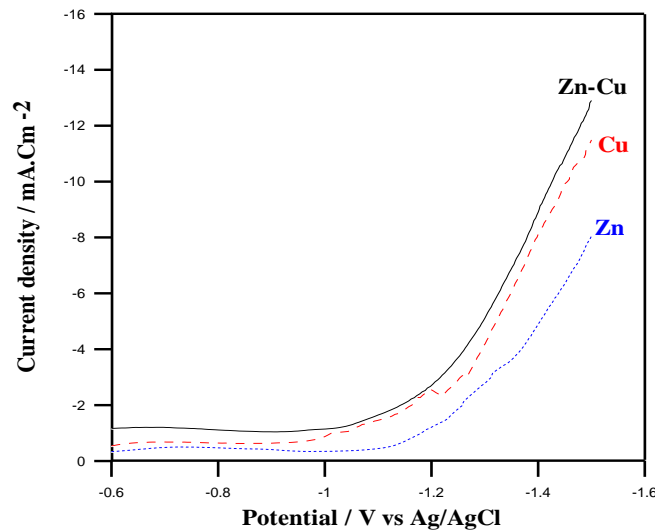
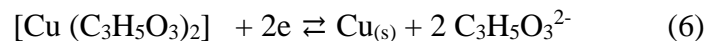
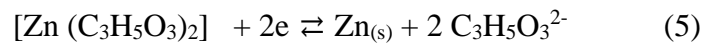


**Figure 1.** Cathodic polarization curves obtained at a temperature of 25 °C and pH 10 for the electrodeposition of copper, zinc, and Cu-Zn. Each solution contains 0.6 M lactic acid and 0.2 M Na<sub>2</sub>SO<sub>4</sub>.

Concentration polarization is often prevalent in the current complex solution as Zn, and Cu is available in these solutions as a lactate complex. The electro-reduction reactions listed below are feasible, with hydrogen evolution occurring due to a separate side reaction [42].



The concentration of the lactate ligand at the cathode surface grows as Zn<sup>2+</sup> and Cu<sup>2+</sup> are discharged, shifting the cathodic polarization towards more negative values.

The partial polarization curves for instantaneous discharge of Zn<sup>2+</sup>, Cu<sup>2+</sup>, and H<sup>+</sup> throughout alloy deposition were calculated utilizing the alloy composition / current curves. The results are shown in Fig. 2. The partial current for hydrogen release is modest, indicating that an alloy with high cathodic current efficacy has been deposited. The partial polarization curve of copper shifts somewhat in the negative direction and approaches that of an alloy, whereas the partial polarization curve of zinc shifts substantially to the negative potential. These findings suggest that copper is a metal that can be easily deposited. This is consistent with the obtained results in the present work.

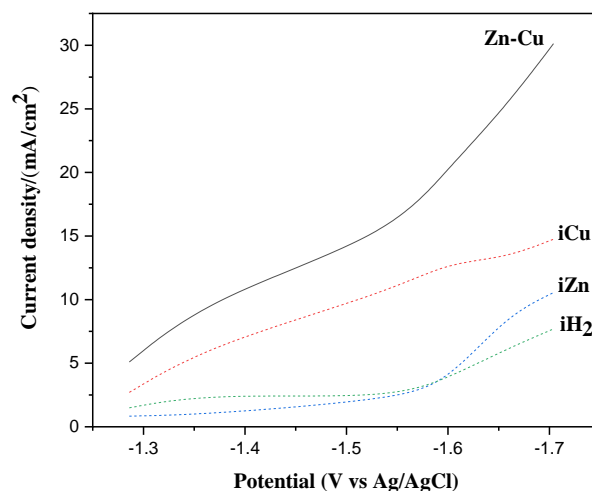


**Figure 2.** Partial current densities for Cu, Zn, and H<sub>2</sub> during the electrodeposition of Cu-Zn alloy.

The effect of the [Zn<sup>2+</sup>] / [Cu<sup>2+</sup>] molar ratio on the overvoltage of Zn-Cu alloy deposition is shown in Fig. 3. As the [Zn<sup>2+</sup>] / [Cu<sup>2+</sup>] ratio declines in the bath, the curves of polarization

shift to increasingly positive values. The concentration of  $\text{Cu}^{2+}$  ions in the tub rises as the molar ratio reduces. Increasing the concentration of  $\text{Cu}^{2+}$  ions at the diffusion layer causes a decrease in the value of cathodic polarization [39].

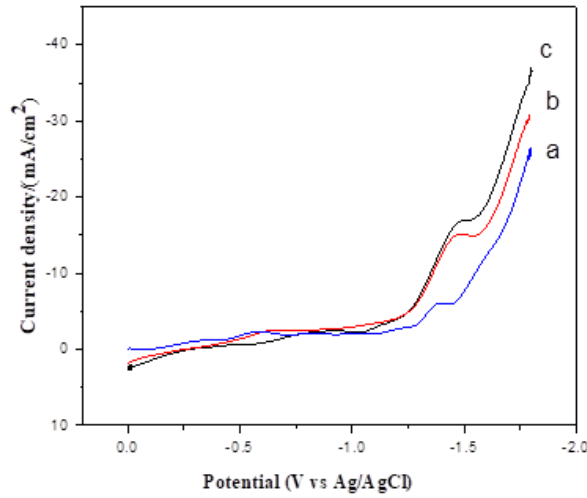


**Figure 3.** Cathodic polarization curves for the deposition of Cu-Zn alloy on steel from a solution with different molar ratios of  $[\text{Zn}^{2+}] / [\text{Cu}^{2+}]$ : (a) 9, (b) 4, and (c) 0.67.

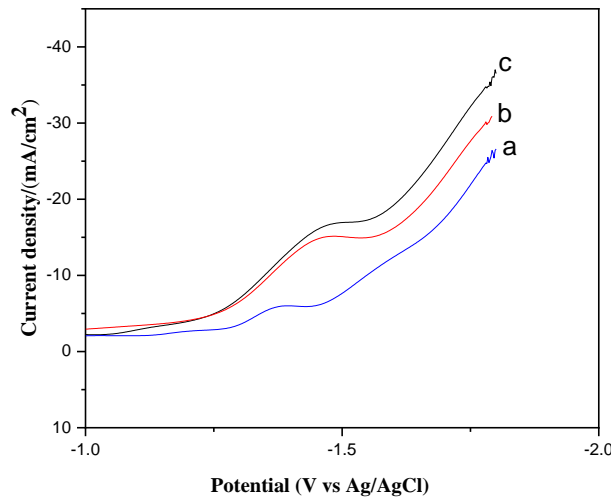


**Figure 4.** Cathodic polarization curves for the deposition of Cu-Zn alloy on steel from a solution containing different concentrations of lactic acid: (a) 0, (b) 1 & (c) 2 M.

Fig. 4 depicts the impact of lactic acid concentration on alloy plating overvoltage. The discharge potential of the alloy shifts to pronounced nobler values as the acid quantity in the bath increases. This behavior might be clarified by adding acid boosts Zn-Cu alloy formation. Furthermore, the addition of lactic acid promotes Zn deposition by complexation and creating a homogeneous catalyst. Abd El-Rehim et al. [43,44] reported similar findings with citrate ions. Moreover, lactate ions can act as a catalyst for Zn-Cu alloy discharge across the steel cathode while not preventing alloy discharge over active sites on the steel surface [45].

Fig. 5 shows how the bath temperature affects the polarization of Zn – Cu alloy plating. The deposition potential of ionic species ( $\text{Zn}^{2+}$ ,  $\text{Cu}^{2+}$ , and  $\text{H}^+$ ) becomes nobler with increasing temperature because polarization decreases. The higher the elevation in temperature, the greater the decrease in cathodic polarization. Because the diffusion rate increases with temperature, the rising temperature will increase the concentration of reducible species in the cathodic diffusion layer. In addition, increasing temperature decreases the activation type of polarization. As the polarization of hydrogen discharge decreases, the evolution of hydrogen becomes more favorable.

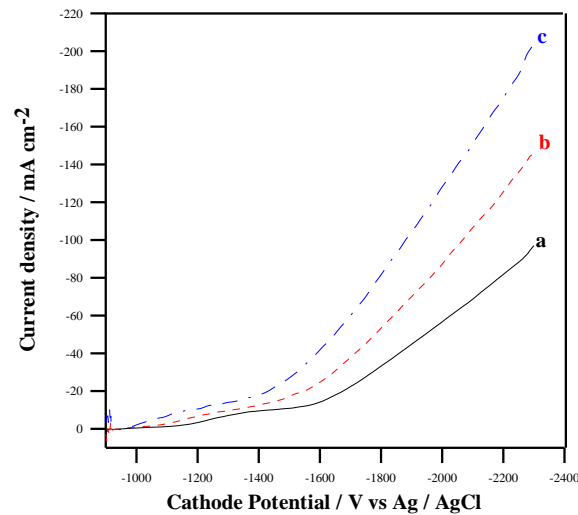


**Figure 5.** Cathodic polarization curves for the deposition of Cu-Zn alloy on steel at different temperatures: (a) 25, (b) 35, and (c) 55 °C.

### 3.2. Zn – Cu electrodeposited alloy composition.

Under different testing conditions, the cathodic current efficacy of the alloy plating (CE), and the zinc % in the alloy are calculated, and the findings are shown in Figs. 6 – 9. The composition reference line (CRL) in these graphs reflects the % of Zn in the tub. For baths with large concentrations of  $\text{Cu}^{2+}$ , the current efficacy of alloy deposition is shown to be high. Depending on the operational parameters and the bath ingredients, current efficiency ranged from 57 to 96 %. Deposition from cyanide baths was reported to be 75%, and from citrate baths to be 70–80% [46]. On the other hand, the deposit has a Zn concentration of 8 to 70%. The deposits' Zn concentration is always lower than the CRL, indicating normal deposition with preferential deposition of copper.

The influence of the  $[\text{Zn}^{2+}] / [\text{Cu}^{2+}]$  molar ratio on the % of Zn in the coating and co-deposition efficacy is shown in Fig. 6. Since the potentials in these conditions are insufficiently negative to reduce  $\text{Zn}^{2+}$  ions, increasing the  $\text{Cu}^{2+}$  amount in the bath significantly diminishes the Zn percent in the deposit. As the  $[\text{Zn}^{2+}] / [\text{Cu}^{2+}]$  molar ratio in the bath rises, so does the co-deposition efficacy.

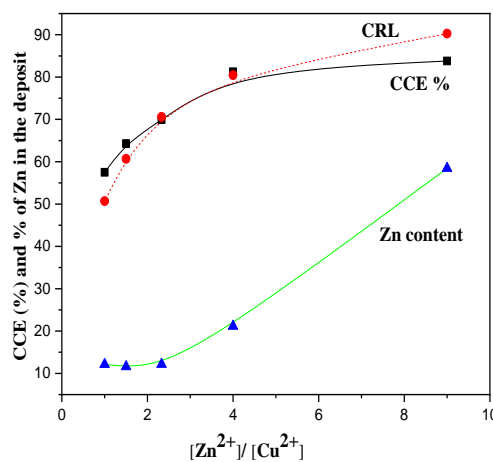


**Figure 6.** The effect of  $[\text{Zn}^{2+}] / [\text{Cu}^{2+}]$  molar ratios on CE of alloy deposition and percentage of Zn in the deposit. CRL represents the percentage of Zn in the bath.

Fig. 7 shows that when the lactic acid concentration rises, the zinc percent in the deposit rises as well, until leveling out. The CE of alloy deposition increases when the concentration

of lactic acid increases from 0.6 to 1.2 M. The CE of alloy deposition diminishes after this value because the deposit falls from the steel's surface.

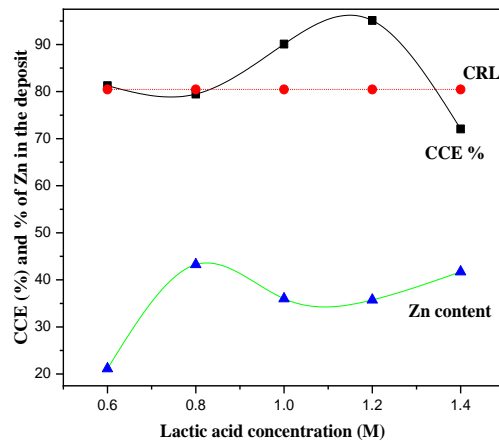


**Figure 7.** Effect of lactic acid concentration on CE of alloy deposition and percentage of Zn in the deposit. CRL represents the percentage of Zn in the bath.

Fig. 8 shows how the depositing current density affects the CE of alloy plating and alloy structure. The figure's data demonstrates that the influence of current density is more complicated. By raising the plating current density from 0.55 to 1.66 mA cm<sup>-2</sup>, the efficacy of co-deposition improves, although the percent of Zn in the coating reduces marginally. When the current density rises, so does the proportion of Zn in the coating. However, cathodic efficacy decreases.

The current density's influence methodology can be examined from two perspectives: diffusion management and cathode potential. In the latter case, as current density rises, the cathode potential shifts to less noble values, and the depositing conditions resemble those depicted by the current–potential curve of the more active metal. This condition should, a priori, raise the fraction of the less noble metal in the deposit. According to conventional diffusion theory, the rate of metal plating has a topmost limit that is dictated by the rate at which its ions may flow across the diffusion layer. The plating rate of a nobler metal is substantially near to its limiting value ( $I_L$ ) than the less noble metal for a given current density. As a result, an increment in current density must have been carried primarily by a faster deposition rate of the less noble metal. It is clear from the data of Fig. 8 and the previous mechanism that the  $I_L$  for Cu plating is primarily 1.66 mA cm<sup>-2</sup>.

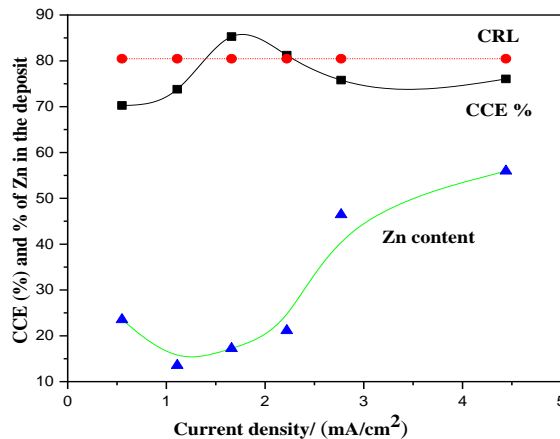


**Figure 8.** Effect of current density on the CE of alloy deposition and percentage of Zn in the deposit. CRL represents the percentage of Zn in the bath.



Increases in c.d. below this value result in a considerable increase in Cu deposition efficiency and a modest drop in Zn deposition efficiency. As a result, one can anticipate an improvement in co-deposition efficiency and a modest drop in the proportion of Zn in the deposit. When the applied current attains the limiting value of Cu deposition, copper ions are depleted in the diffusion layer, causing the deposition rate of Zn to increase (the less noble metal). As a result of a big fall in Cu efficiency and a smaller increase in Zn efficiency, the Zn percent in the deposit increases, but the co-deposition efficiency declines.

An increment in the temperature from 10 to 55 °C reduces the Zn % in the coating and enhances the CE of alloy plating, as shown in Fig. 9. The efficacy of co-deposition reduces dramatically as the temperature rises. As the rates of both diffusion and convection rise with temperature, elevating bath temperature increases the number of reducible species in the cathodic diffusion layer. Increased deposition of copper (nobler metal), which deposits preferentially under these conditions, is favored by an increment in reducible species amount at the solution–cathode boundary. As a result, as the temperature rises, the Zn % in the deposit falls. Because of the substantial rise in Cu efficiency and the smaller reduction in Zn efficiency, the CE of alloy deposition increases.

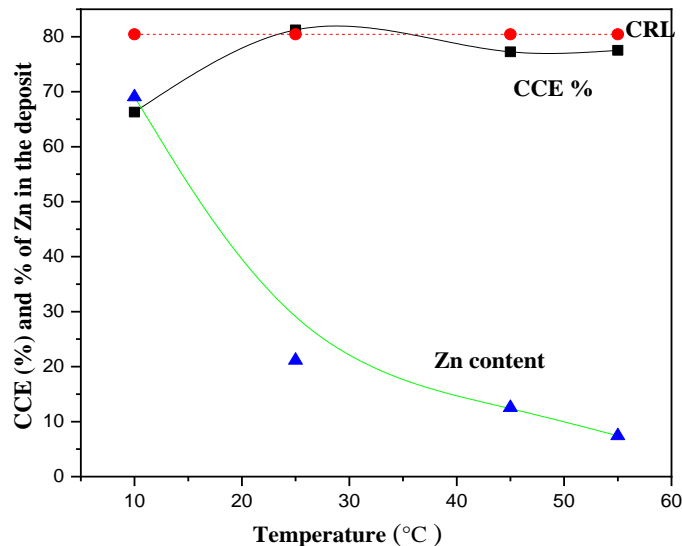


**Figure 9.** Effect of temperature on the CE of alloy deposition and percentage of Zn in the deposit. CRL represents the percentage of Zn in the bath.

### 3.3. Throwing power (TP) and throwing index (TI) tests.

The variation of the throwing power and throwing index of the alkaline lactate baths for electroplating of Zn – Cu with the bath composition and different operating variables were examined. The experimental data is shown in Table 1. According to the results, the lactate bath for Zn – Cu electroplating does have a high TP.

As shown in Table 1, increasing the  $[Zn^{2+}] / [Cu^{2+}]$  molar ratio in the bath improves T.P and T.I significantly by decreasing cathodic polarization. On the other hand, increased lactic acid concentration reduces both TP & TI.

Increasing the deposition current density reduces both the TP & TI. Increasing the tub's temperature from 25 to 55 °C slightly decreases the throwing power, as shown in Table 1. This impact could be thought to be due to the depolarizing impact of higher temperatures, even though rising temperatures increase electrolyte conductivity. This result indicates that the depolarization effect is more effective.



**Table 1.** The influence of bath constituents and plating parameters on the throwing power and throwing index of a copper-zinc alloy electroplating.

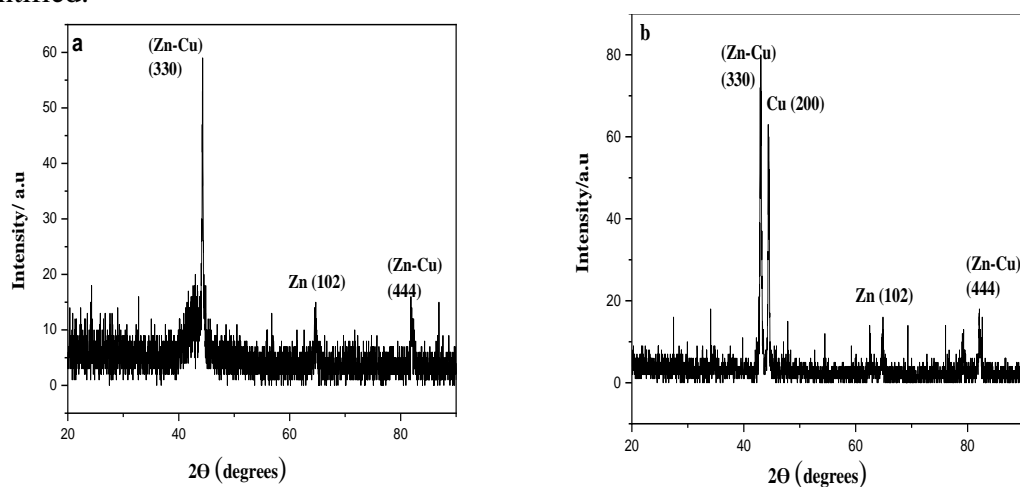
Bath composition				Plating variables			T.I	T.P (%)
Copper sulfate (M)	Zinc sulfate (M)	Lactic acid (M)	Sodium sulfate (M)	c.d. (mA cm <sup>-2</sup> )	Time (min)	Temp (°C)		
0.18	0.02	0.6	0.2	2.22	20	25	64.5	96.9
0.16	0.04	0.6	0.2	2.22	20	25	2.9	49.3
0.18	0.02	2	0.2	2.22	20	25	3.8	58.1
0.18	0.02	0.6	0.2	4.44	20	25	11.7	84.2
0.18	0.02	0.6	0.2	2.22	20	55	7.8	77.1

### 3.4. Structure and morphology of the depositing alloy.

Visual observations illustrate that the Zn – Cu deposits obtained from the alkaline lactate bath are compact, bright, and grey to reddish-brown in appearance with good adhesion to the steel substrate. The luminance of the deposit increases as the plating current density or Cu<sup>2+</sup> content of the bath increases. The deposit becomes darker as the temperature or Zn<sup>2+</sup> content of the bath rises.

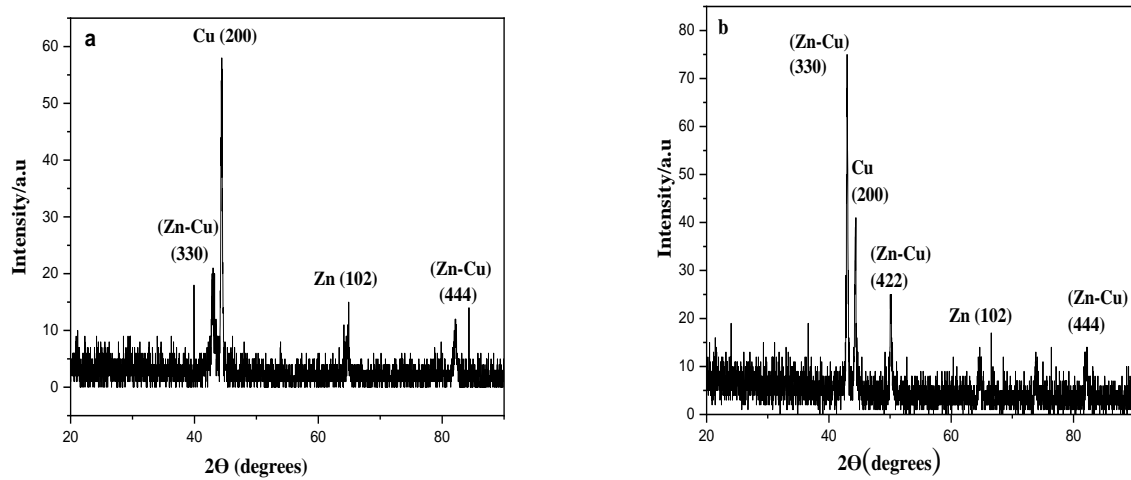
XRD was conducted out on a few Zn –Cu alloy plates electroplated from tubs under varying deposition conditions. The results are depicted in Figs. 10 and 11. The experimentally obtained crystal planes (hkl) were matched to the predicted values for the phases outlined in JCPDS. Regardless of the bath constituents or electroplating parameters, all deposits are crystalline and composed of face-centered cubic (FCC) Cu<sub>5</sub>Zn<sub>8</sub> phase [47]. These copper-rich alloys can be thought of as having a copper lattice with some copper atoms replaced by zinc atoms. The diffractograms also revealed that the alloy deposits have a favored orientation of (330). The finding of a fixed angle for the (330) planes is believed to be because copper and zinc share identical lattice parameters and coherent interfaces between Cu and Zn phases [48].

Fig. 10 depicts the impact of current density on the XRD spectra of electroplated Zn – Cu alloy. At reduced current density, 2.22 mA cm<sup>-2</sup>, the electroplated alloy exemplifies a (330) strong intensity diffraction peak and a (102) relatively weak intensity diffraction peak, in addition to the diffraction peak (444), Fig. 10 a. At 4.44 mA cm<sup>-2</sup>, the intensity of the (330) plane increases significantly, while the intensity of the (102) plane decreases slightly, as shown in Fig. 10 b. It is worth noting that a new diffraction (200) plane for Cu metal has been identified.



**Figure 10.** X-ray diffraction patterns of electrodeposited Cu-Zn alloy obtained at different current densities: (a) 2.22, and (b) 4.44 mAcm<sup>-2</sup>.

The intensity of the plane (330) increases as the bath temperature rises from 25 to 55°C, whereas the intensity of the Cu peak (200) decreases; additionally, the intensity of the peak (444) is unaffected, Fig. 11.



**Figure 11.** X-ray diffraction patterns of electrodeposited Cu-Zn alloy obtained at different temperatures: (a) 5, and (b) 55 °C.

As shown in Fig. 12, EDX analysis confirmed the existence of both copper and zinc metals in the deposit. The presence of iron metal in the pattern indicates that the deposited layer has a small thickness.

SEM was used to examine the microstructural and morphological growth characteristics of an as-deposited Zn - Cu alloy, developed under varied plating and running conditions. Figs. 13&14 show some of the SEM images. The deposits formed at low current density are compact and smooth, as shown in Fig. 13 a. The surface seemed to be made of tightly packed spheres. Upping the current density causes the forming of fine-grained and leveled deposits, Fig. 13 b. An increment could cause the structural change in cathodic polarization that speeds up nucleation and facilitates the forming of fine-grained coatings [49].

Fig. 14 depicts the impact of temperature on the morphological features of an electroplated Zn–Cu alloy. Low temperatures encourage the forming of uniform, soft, leveled, and compact coatings, Fig. 14 a. However, higher temperatures enhance the forming of limited spherical grains that cover the whole substrate and have left some empty spaces, Fig. 14 b. This sort of behavior could be related to the limited cathodic efficacy of Zn–Cu plating at elevated temperatures and the rapid evolution of H<sub>2</sub> gas [50].

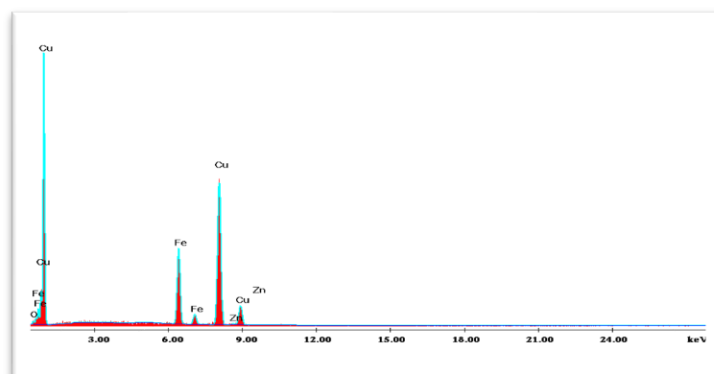


**Figure 12.** EDX patterns of electrodeposited Cu-Zn alloy obtained from a bath containing 0.16 M ZnSO<sub>4</sub>·7H<sub>2</sub>O, 0.04 M CuSO<sub>4</sub>·5H<sub>2</sub>O, 0.6 M lactic acid, and 0.2 M Na<sub>2</sub>SO<sub>4</sub>, at pH10, time 20 min, c.d. 2.22 mA cm<sup>-2</sup> and 55 °C.

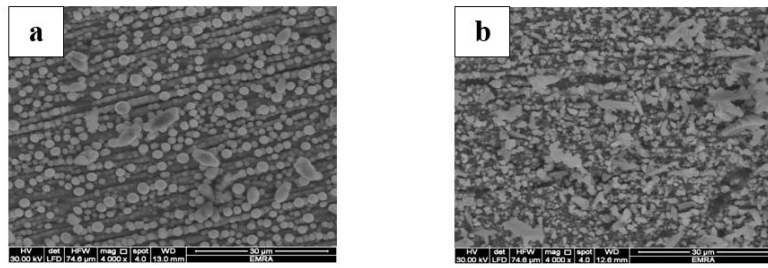


**Figure 13.** Scanning electron micrographs of electrodeposited Cu-Zn alloy obtained at different current densities: (a) 2.22 and (b) 4.44 mA cm<sup>-2</sup>.

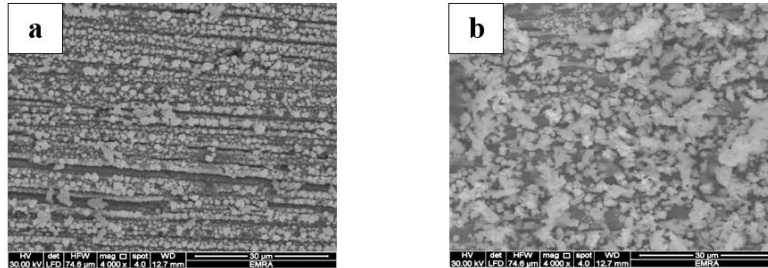


**Figure 14.** Scanning electron micrographs of electrodeposited Cu-Zn alloy obtained at different temperatures: (a) 25 and (b) 55 °C.

#### 4. Conclusions

The electrodeposition of brass alloy onto steel coupons from aqueous solutions comprising lactate ions was studied under different operational parameters. The deposition was done in a bath that contained CuSO<sub>4</sub>·5H<sub>2</sub>O, ZnSO<sub>4</sub>·7H<sub>2</sub>O, and CH<sub>3</sub>CHOHCOOH & Na<sub>2</sub>SO<sub>4</sub>. An increment in the lactic acid concentration in the plating bath shifts the deposition potential of brass alloy to more positive values. In addition, increasing the bath temperature or decreasing the [Zn<sup>2+</sup>] / [Cu<sup>2+</sup>] molar ratio in the bath facilitates the deposition of brass alloy. The Zn-Cu alloy deposition has a high current efficacy. The deposition of Zn-Cu alloy belongs to the normal category. The efficacy of alloy deposition increases as the [Zn<sup>2+</sup>] / [Cu<sup>2+</sup>] molar ratio increases in solution. The CE of alloy deposition increases when the lactic acid concentration is increased from 0.6 to 1.2 M. The deposited brass alloys are rich in copper. The Zn % of the alloy increases with applied current density, [Zn<sup>2+</sup>] / [Cu<sup>2+</sup>] molar ratio, and lactic acid concentration; however, it tends to decrease with rising temperature. The brightness of the deposits increases as the plating current density or Cu<sup>2+</sup> content of the bath increments. The deposits have a Cu<sub>5</sub> Zn<sub>8</sub> phase structure with a small thickness. The alkaline lactate bath for brass electroplating possesses good throwing power and throwing index.

#### Funding

This research was funded by Taif University Researchers Supporting, Taif, Saudi Arabia; grant number (TURSP – 2020/136).

#### Acknowledgments

We thank all the staff of the Department of Chemistry at the University of Suez Canal for their support.

#### Conflicts of Interest

The authors declare no conflict of interest.

## References

1. Ballesteros, J.C.; Torres-Martínez, L.M.; Juárez-Ramírez, I.; Trejo, G.; Meas, Y. Study of the electrochemical co-reduction of Cu<sup>2+</sup> and Zn<sup>2+</sup> ions from an alkaline non-cyanide solution containing glycine. *Journal of Electroanalytical Chemistry* **2014**, *727*, 104–112, <https://doi.org/10.1016/j.jelechem.2014.04.020>.
2. Lowenheim, F.A. *Modern electroplating*. 3rd ed.: John-Wiley & Sons: New York, USA, **1974**.
3. Brenner, A. *Electrodeposition of Alloys*. Volume 1: Academic Press: New York, USA, **1963**; pp. 411–475, <https://doi.org/10.1002/bbpc.19640680319>.
4. Musa, A.; Slaiman, Q.; Kadhum, A.; Kadhum, H.; Takriff, M. Effects of agitation, current density and cyanide concentration on Cu-Zn alloy electroplating. *Eur. J. Sci. Res.* **2008**, *22*, 517–524.
5. Dudek, D.A.; Fedkiw, P.S. Electrodeposition of copper from cuprous cyanide electrolyte: II. Current distribution on a rotating disk. *Journal of Electroanalytical Chemistry* **1999**, *474*, 31–42, [https://doi.org/10.1016/S0022-0728\(99\)00300-9](https://doi.org/10.1016/S0022-0728(99)00300-9).
6. Horner, J. Cyanide copper plating. *Plat. Surf. Finish.* **1997**, *84*, 52–57.
7. Safranek, W.H. *The properties of electrodeposited metals and alloys*. 2<sup>nd</sup> ed.: American Electroplaters and Surface Finishers Society: Orlando, FL, USA, **1986**; pp. 550, <https://doi.org/10.1149/1.2134416>.
8. Davis, J. *Copper and copper alloys*. ASM International, **2001**.
9. Hacıbrahimoglu, M.; Yavuz, A.; Öztaş, M.; Bedir, M. Electrochemical and structural study of zinc-rich brass deposited from pyrophosphate electrolyte onto the carbon steel. *Digest Journal of Nanomaterials and Biostructures* **2016**, *11*, 251–262.
10. Vivegnis, S.; Krid, M.; Delhalle, J.; Mekhalif, Z.; Renner, F.U. Use of pyrophosphate and boric acid additives in the copper-zinc alloy electrodeposition and chemical dealloying. *Journal of Electroanalytical Chemistry* **2019**, *848*, <https://doi.org/10.1016/j.jelechem.2019.113310>.
11. Silva, F.L.G.; do Lago, D.C.B.; D'Elia, E.; Senna, L.F. Electrodeposition of Cu–Zn alloy coatings from citrate baths containing benzotriazole and cysteine as additives. *Journal of Applied Electrochemistry* **2010**, *40*, 2013–2022, <https://doi.org/10.1007/s10800-010-0181-z>.
12. Tintelecan, M.; Iluțiu-Varvara, D.-A.; Alabanda, O.R.; Sas-Boca, I.M. A technical version of achieving a brass coated surface on steel wires. *Procedia Manuf.* **2020**, *46*, 12–18, <https://doi.org/10.1016/j.promfg.2020.03.003>.
13. De Filippo, D.; Rossi, A.; Atzei, D. A tartrate-based alloy bath for brass-plated steel wire production. *Journal of Applied Electrochemistry* **1992**, *22*, 64–72, <https://doi.org/10.1007/BF01093013>.
14. Barros, K.S.; Ortega, E.M.; Pérez-Herranz, V.; Espinosa, D.C.R. Evaluation of brass electrodeposition at RDE from cyanide-free bath using EDTA as a complexing agent. *J. Electroanal. Chem.* **2020**, *865*, <https://doi.org/10.1016/j.jelechem.2020.114129>.
15. Ramírez, C.; Calderón, J.A. Study of the effect of triethanolamine as a chelating agent in the simultaneous electrodeposition of copper and zinc from non-cyanide electrolytes. *J. Electroanal. Chem.* **2016**, *765*, 132–139, <https://doi.org/10.1016/j.jelechem.2015.06.003>.
16. Ibrahim, M.A.M.; Bakdash, R.S. New cyanide-free ammonia bath for brass alloy coatings on steel substrate by electrodeposition. *Int. J. Electrochem. Sci.* **2015**, *10*, 9666–9677.
17. Fujiwara, Y.; Enomoto, H. Electrodeposition of Cu-Zn alloys from glucoheptonate baths. *Surface and Coatings Technology* **1988**, *35*, 101–111, [https://doi.org/10.1016/0257-8972\(88\)90061-8](https://doi.org/10.1016/0257-8972(88)90061-8).
18. Ibrahim, M.A.M.; Bakdash, R.S. Copper-rich Cu–Zn alloy coatings prepared by electrodeposition from glutamate complex electrolyte: morphology, structure, microhardness and electrochemical studies. *Surf. Interfaces* **2020**, *18*, <https://doi.org/10.1016/j.surfin.2019.100404>.
19. Rashwan, S.M. Electrodeposition of Zn–Cu coatings from alkaline sulphate bath containing glycine. *Transactions of the IMF* **2007**, *85*, 217–224, <https://doi.org/10.1179/174591907X216440>.
20. Ghorbani, M.; Mazaheri, M.; Khangholi, K.; Kharazi, Y. Electrodeposition of graphite-brass composite coatings and characterization of the tribological properties. *Surf. Coat. Technol.* **2001**, *148*, 71–76, [https://doi.org/10.1016/S0257-8972\(01\)01322-6](https://doi.org/10.1016/S0257-8972(01)01322-6).
21. Das, S.; Jena, S.; Banthia, S.; Mitra, A.; Das, S.; Das, K. Novel pulse potentiostatic electrodeposition route for obtaining pure intermetallic Cu<sub>5</sub>Zn<sub>8</sub>-CuZn composite coating using glycerol-NaOH based electrolyte with advanced scratch resistance and anti-corrosive properties. *Journal of Alloys and Compounds* **2019**, *792*, 770–779, <https://doi.org/10.1016/j.jallcom.2019.04.068>.
22. Chun-Yao, W.; Yao-Tien, T.; Jing-Chie, L.; Yong-Jie, C.; Yean-Ren, H. Effect of [Zn<sup>2+</sup>]/[Cu<sup>2+</sup>] ratio of the bath on the composition and property of Cu–Zn alloy micropillars prepared using microanode-guided electroplating. *Electrochim. Acta* **2021**, *375*, <https://doi.org/10.1016/j.electacta.2021.13796>.
23. Chongyan, C.; Lifeng, D.; Qiang, L.; Ruonan, W.; Jinxia, Y.; Qi, W.; Yanfeng, X.; Hongdao, L.; Yulan, N. Effects of four carboxyl-containing additives on imitation gold electroplating Cu-Zn-Sn alloys in an HEDP system. *J. Solid State Electrochem.* **2021**, *25*, 1361–1371, <https://doi.org/10.1007/s10008-021-04914-0>.
24. Amina, D.; Leila, D.; Jean-Yves, H.; Patrice, B.; Wafa, S.; El Mustafa, R. CuZn electrodeposition in cyanide-free electrolytes: Influence of citrate/metal ratio and pH on simultaneous copper and zinc reduction kinetics and alloy composition control. *J. Electrochem. Soc.* **2020**, *167*, <https://dx.doi.org/10.1149/1945-7111/ab819b>.



25. Yassine, S.; Sghir, C.; Jihane, T.; Mohammed, C. Electrodeposition of Cu-Zn-Sn coating in citrate medium dissolution. *Mediterr. J. Chem.* **2020**, *9*, 456-467, <https://dx.doi.org/10.13171/mjc9601071073ys>.
26. Tintelecan, M.; Iluțiu-Varvara, D.; Alabanda, O.; Sas-Boca, I. A technical version of achieving a brass coated surface on steel wires. *Procedia Manuf.* **2020**, *46*, 12–18.
27. García-Mintegui, C.; Córdoba, L.C.; Buxadera-Palomero, J.; Marquina, A.; Jiménez-Piqué, E.; Ginebra, M.-P.; Cortina, J.L.; Pegueroles, M. Zn-Mg and Zn-Cu alloys for stenting applications: From nanoscale mechanical characterization to in vitro degradation and biocompatibility. *Bioactive Materials* **2021**, *6*, 4430-4446, <https://doi.org/10.1016/j.bioactmat.2021.04.015>.
28. Cercado, B.; Teran, A.; Ballesteros, J.C.; Vázquez-Arenas, J.; Lara, R.H.; Țălu, Ș.; Méndez-Albores, A.; Trejo, G. Nucleation and growth mechanism of Cu-Zn/AgNPs composite coatings at different concentrations of silver nanoparticles (AgNPs) in solution. *Electrochimica Acta* **2021**, *390*, <https://doi.org/10.1016/J.ELECTACTA.2021.138867>.
29. Ezer, C.; Nikolay, D. Electrodeposition of Zn-rich  $Cu_xZn_{(1-x)}$  films with controlled composition and morphology. *J. Electrochem. Soc.* **2021**, *168*, <https://doi.org/10.1149/1945-7111/AC0A25>.
30. Aimin, L.; Zhongning, S.; Ramana, G. Mechanism study of Cu-Zn alloys electrodeposition in deep eutectic solvents. *Ionics* **2020**, *26*, 3161–3172, <https://doi.org/10.1007/s11581-019-03418-2>.
31. Geramipour, F.; Mousavi, S.; Shooshtari, H. Effect of shaped waveform on structure and electrochemical corrosion behavior of pulse electrodeposited Ni-Cu alloy coatings. *J. Surf. Coat. Technol.* **2021**, *424*, <https://doi.org/10.1016/j.surfcoat.2021.127643>.
32. Christine, A.; Louis, H.; Tanujjal, B. Cyanide-free environment-friendly alternative to copper electroplating for zinc die-cast alloys. *Environ. Sci. Pollut. Res.* **2021**, *28*, 38065–38073, <https://doi.org/10.1007/s11356-021-13398-4>.
33. Kayo, S.; Tatiana, S.; Valentín, P.; Denise, C. Treatment of cyanide-free wastewater from brass electrodeposition with EDTA by electrodialysis: evaluation of under limiting and over limiting operations. *Membranes* **2020**, *10*, <https://doi.org/10.3390/membranes10040069>.
34. Antonina, M.; Ihor, O. Dissolution of zinc-enriched phases during layer-by-layer deposition of Cu-Zn thin films. Conference: 2020 IEEE 40th International conference on electronics and nanotechnology (ELNANO), Kyiv, Ukraine, 22-24 April **2020**, <https://doi.org/10.1109/ELNANO50318.2020.9088876>.
35. Cheng, J.; Ding, L.; Li, Q.; Chen, C.; Wang, R.; Kong, X.; Song, Z.; Zhao, X.; Niu, Y. Effect of hydroxyl-containing additives on the codeposition of Cu-Zn-Sn alloys. *Journal of Applied Electrochemistry* **2020**, *50*, 475-488, <https://doi.org/10.1007/s10800-020-01405-4>.
36. Enrico, B.; Calisi, N.; Capaccioli A.; Laura, C. Electrodeposited white bronzes on brass: Corrosion in 3.5 % sodium chloride solution. *Corros. Sci.* **2020**, *175*, <https://doi.org/10.1016/j.corsci.2020.108898>.
37. Qiao, X.; Li, H.; Zhao, W.; Li, D. Effects of deposition temperature on electrodeposition of zinc-nickel alloy coatings. *Electrochim. Acta* **2013**, *89*, 771–777, <https://doi.org/10.1016/j.electacta.2012.11.006>.
38. Abd El Rehim, S.S.; Abd El Wahaab, S.M.; Ibrahim, M.A.M.; Dankeria, M.M. Electroplating of cobalt from aqueous citrate baths. *Journal of Chemical Technology & Biotechnology* **1998**, *73*, 369-376, [https://doi.org/10.1002/\(SICI\)1097-4660\(199812\)73:4<369::AID-JCTB971>3.0.CO;2-P](https://doi.org/10.1002/(SICI)1097-4660(199812)73:4<369::AID-JCTB971>3.0.CO;2-P).
39. Kamel, M. Anomalous codeposition of Co-Ni: Alloys from gluconate baths. *Journal of Applied Electrochemistry* **2007**, *37*, 483-489, <https://doi.org/10.1007/s10800-006-9279-8>.
40. Kamel, M. M.; Alzahrani, E.; Ibrahim, I. S.; Rashwan, S. M. Electrodeposition of well-crystalline Ni-Co alloy thin films on steel substrates from aqueous solutions containing citrate anions. *Int. J. Electrochem. Sci.* **2021**, *16*, 1-22, <https://doi.org/10.20964/2021.09.18>.
41. Portanova, R.; Lajunen, L. H. J.; Tolazzi, M.; Piispanen, J. Critical evaluation of stability constants for  $\alpha$ -hydroxycarboxylic acid complexes with protons and metal ions and the accompanying enthalpy changes. Part II. Aliphatic 2-hydroxycarboxylic acids (IUPAC Technical Report). *Pure Appl. Chem.* **2003**, *75*, 495-540, <https://doi.org/10.1351/pac200375040495>.
42. Kamel, M.M.; Anwar, Z.M.; Abdel-Salam, I.T.; Ibrahim, I.S. Electrodeposition of nanocrystalline Ni – Cu alloy from environmentally friendly lactate bath. *J. Surf. Interface. Anal.* **2014**, *46*, 442–448.
43. Abd El Rehim, S.S.; Abd El Wahab, S.; Rashwan, S.M.; Anwar, Z.M. Electrodeposition of Copper-Nickel Alloys from a Citrate Bath Containing Boric Acid. *Transactions of the IMF* **1999**, *77*, 242-245, <https://doi.org/10.1080/00202967.1999.11871292>.
44. El-Rehim, S.S.; El-Wahab, S.M.; Rashwan, S.M.; Anwar, Z.M. Electroplating of a Co-Cu alloy from a citrate bath containing boric acid. *Journal of Chemical Technology & Biotechnology* **2000**, *75*, 237-244, [https://doi.org/10.1002/\(SICI\)1097-4660\(200003\)75:3<237::AID-JCTB189>3.0.CO;2-I](https://doi.org/10.1002/(SICI)1097-4660(200003)75:3<237::AID-JCTB189>3.0.CO;2-I).
45. Ibrahim, M.A.M.; Bakdash, R.S. New non-cyanide acidic copper electroplating bath based on glutamate complexing agent. *Surface and Coatings Technology* **2015**, *282*, 139-148, <https://doi.org/10.1016/j.surfcoat.2015.10.024>.
46. Ibrahim, M.; Ismail, E.; Bakdash, R. Copper-rich copper-zinc alloy coatings prepared by electrodeposition from glutamate complex electrolyte: current efficiency, Tafel kinetics and throwing power. *Transactions of the IMF* **2019**, *97*, 237-246, <https://doi.org/10.1080/00202967.2019.1644764>.
47. Smith, D. *JCPDS Grant-in-Aid Report*. The Pennsylvania State Univ. **1973**.

48. Bradley, P. E.; Landolt, D. Pulse-plating of copper–cobalt alloys. *Electrochim. Acta.* **1999**, *45*, 1077–1087, [https://doi.org/10.1016/S0013-4686\(99\)00301-1](https://doi.org/10.1016/S0013-4686(99)00301-1).
49. Maciej, A.; Łatanik, N.; Sowa, M.; Matuła, I.; Simka, W. Electrodeposition of Copper and Brass Coatings with Olive-Like Structure. *Materials* **2021**, *14*, <https://doi.org/10.3390/ma14071762/>.
50. Oulmas, C.; Mameri, S.; Boughrara, D.; Kadri, A.; Delhalle, J.; Mekhalif, Z.; Benfedda, B. Comparative study of Cu–Zn coatings electrodeposited from sulphate and chloride baths. *Heliyon* **2019**, *5*, <https://doi.org/10.1016/j.heliyon.2019.e02058>.